Adsorption/Desorption Studies of NO$_x$ on Well-Mixed Oxides Derived from Co−Mg/Al Hydrotalcite-like Compounds

Jun Jie Yu,[†] Zheng Jiang,[†] Ling Zhu,[†] Zheng Ping Hao,*,[†] and Zhi Ping Xu*,[‡]

Research Center for Eco-Environmental Sciences, Chinese Academy of Sciences, Beijing 100085, PR China, and Australian Research Council (ARC) Centre for Functional Nanomaterials, School of Engineering, The University of Queensland, Brisbane QLD 4072, Australia

Co$_x$Mg$_{3-x}$/Al hydrotalcite-like compounds (where x = 0.0, 0.5, 1.0, 1.5, 2.0, 2.5, 3.0) were synthesized by the coprecipitation method and characterized by the XRD and TGA techniques. Incorporation of Co for x = 0.0−3.0 gradually decreased the transformation temperature of the hydrotalcites to the corresponding oxides from 444 to 246 °C and also decreased the surface area from 162.7 to 21.6 m^2/g upon calcination at 800 °C for 4 h in air. The resultant oxide was generally composed of a poor MgO phase and a spinel phase, with more spinel phase at higher Co incorporation. The derived oxides were tested as the storage/reduction catalysts for NO$_x$ adsorption/desorption. The storage capacity for NO$_x$ was highly dependent on the catalyst composition and storage temperature. In general, more NO$_x$ was stored at lower temperature (100 °C) than that at higher temperature (300 °C), and tertiary catalysts (x = 0.5−2.5) stored more NO$_x$ than binary catalyst (x = 0.0 or 3.0). The catalytic conversion of NO to NO$_2$ and the catalytic decomposition of NO$_x$ were observed on the tertiary catalysts during NO$_x$ adsorption at 300 °C, which was highly related to the loading of cobalt. The reducibility of catalysts was determined by TPR experiments, and the reduction of cobalt cations started at 150−200 °C in H$_2$. In situ IR spectra of catalysts adsorbing NO$_x$ revealed that the major NO$_x$ species formed on the catalysts were various kinds of nitrites and nitrates, together with some forms of dimers, such as N$_2$O$_2$$^{2-}$ and N$_2$O$_4$ (or NO$^+$NO$_3$$^-$). The storage/reduction mechanism and the function of Co in the mixed oxides are proposed and discussed on the basis of these observations.

Introduction

Various nitrogen oxides (NO$_x$), generally produced in the combustion of fossil fuels, are the major pollutants in air that cause some environmental problems, such as photochemical smog and acid rain, as well as some human diseases, such as asthma.[1] Thus, there is a growing need to reduce emissions of NO$_x$ from automobile combustion, mainly via catalytic decomposition to environmentally friendly N$_2$ and O$_2$. In fact, Pt-Rh-based three-way catalysts (TWCs) can effectively convert NO$_x$ to N$_2$ under conditions of a stoichiometric air-to-fuel ratio.[1,2] However, the general requirement of more fuel-efficient gasoline engines due to limited fossil fuel resources on the earth drives car manufacturers to develop lean-burn engines that combust fuel more efficiently under excess oxygen.[3] The presence of excess oxygen in the exhaust severely reduces the activity of three-way catalysts for NO$_x$ decomposition.[4] Therefore, catalysts that can effectively reduce the NO$_x$ amount in the presence of excess oxygen have now been widely sought, among which NO$_x$ storage/reduction (NSR) catalytic treatment seems a more promising approach to NO$_x$ removal in excess oxygen.[5,6]

NO$_x$ storage/reduction technology is used in engines that alternately operate under lean-burn and rich-burn conditions.[7,8] Under lean-burn conditions, NO is oxidized and is stored on the catalyst. When the engine is switched to conditions with a stoichiometric air-to-fuel ratio, i.e., rich-burn conditions, NO$_x$ species are released and subsequently reduced by hydrocarbons and carbon monoxide.[9,10] A model NO$_x$ storage/reduction catalyst comprises three major components: a high-surface-area support material (e.g., γ-Al$_2$O$_3$), a NO$_x$ storage component containing alkali or alkaline earth metals (e.g., Ca, Sr, Ba, K, or Na), and a noble metal (e.g., Pt, Rh, or Pd) as the catalytic redox component.[9−12] These storage/reduction catalysts are efficient at removing NO$_x$ under lean-rich cycles in the absence of SO$_2$. Nevertheless, a problem is that SO$_2$ generated in trace amounts in the exhaust dramatically deactivates the storage/reduction catalysts,[13] which, together with the high expense of noble metals, demands the development of inexpensive and SO$_2$-tolerant storage/reduction catalysts with similar or better storage/reduction performances.

In sharp contrast to the abundant research on the improvement of the model storage/reduction catalyst Pt−Ba/Al$_2$O$_3$,[9−19] such as introducing other components, including Fe, Ce, Cu, and Ni, the search for other alternative catalysts seems to draw less attention.[10,12,17,18,20−26] Perovskites[10,20−23] and zeolites[24] are the primary candidates that show potential as alternative NSR catalysts. Recently, a type of well-mixed and well-dispersed oxides derived from hydrotalcite-like compounds has received considerable attention in the search for alternative NSR catalysts.[12,17,18,25,26]

Hydrotalcite-like compounds (HTlcs), also known as anionic clays or layered double hydroxides (LDHs), are multifunctional materials that are widely used as adsorbents, ion exchangers, base catalysts, and precursors of well-mixed oxides for various

---

* Corresponding authors. Tel.: +86-10-62849194 (Z.P.H.), 61-7-33469973 (Z.P.X.). Fax: +86-10-62923564 (Z.P.H.), 61-7-33656074 (Z.P.X.). E-mail: zpinghao@mail.rcees.ac.cn (Z.P.H.), zhipingx@cheque.uq.edu.au (Z.P.X.).
† Chinese Academy of Sciences.
‡ The University of Queensland.

catalytic applications.[27,28] HTlcs are a large family of mixed hydroxides and can be chemically expressed by the general formula $[M^{II}_{1-x}M^{III}_x(OH)_2]^{x+}(A^{n-})_{x/n}\cdot mH_2O$, where M^{II} represents any divalent metal cation, M^{III} any trivalent metal cation, and A^{n-} an anion (inorganic or organic).[27,28] HTlcs can contain metal cations of more than two types, which leaves vast flexibility for the better selection of various cations in these materials for NSR catalyst development. For example, in a mixed oxide derived from an M–MgAl HT compound, Al_2O_3 acts as the support; MgO acts as a NO_x storage component; and M (M^{II} and/or M^{III}) can act as the active component for promoting storage of NO_x, conversion of NO_x to N_2 and O_2, and reduction of NO_x with carbon monoxide and hydrocarbons. In fact, Cu-containing calcined MgAl HTlcs have been found to be active and selective catalysts of NO_x removal.[17,18,29] Our recent studies[30,31] show that these HTlc-derived catalysts perform well for NO_x storage/reduction, especially at low temperatures. Taking into account the fact that cobalt species are active components for NO_x removal and decomposition,[32,33] we prepared a series of Co–Mg/Al mixed oxide catalysts from the corresponding HTlc precursors upon calcination. These mixed oxide catalysts were tested as storage/reduction catalysts of mixed NO and NO_2 gases at 100 and 300 °C. The storage amount of NO_x was very much related to the catalyst composition, and there should be an optimum NSR catalyst with a careful tradeoff of the Co/Mg ratio in the precursor. The storage/reduction mechanism of NO_x on these catalysts and the effect of cobalt in these processes were further proposed on the basis of the in situ IR spectra and adsorption/desorption experimental data.

Experimental Section

Materials Preparation. Various Co_xMg_{3-x}/Al hydrotalcite-like compounds with $(Co^{2+} + Mg^{2+})/Al^{3+}$ molar ratio fixed at 3.0 were prepared with a constant-pH coprecipitation method where x was set at 0.0, 0.5, 1.0, 1.5, 2.0, 2.5, and 3.0 (denoted as xCoMA-HT). Briefly, a mixed salt solution (100 mL) and a mixed basic solution (100 mL) were simultaneously added dropwise into 100 mL of doubly distilled water within 1 h at constant pH (10 ±0.5) under vigorous mechanical stirring. The salt solution with a total metal concentration of 1.0 M contains suitable amounts of $Mg(NO_3)_2\cdot 6H_2O$ (>99%, Yili Company), $Co(NO_3)_2\cdot 6H_2O$ (>99%, Jinke Company), and $Al(NO_3)_3\cdot 9H_2O$ (>99%, Yili Company), and the basic solution contains NaOH (>96%, Beihua Company) and Na_2CO_3 (>99.8%, Beihua Company) with $[OH^-]/[CO_3^{2-}] = 16$ and $[OH^-]/[Al^{3+}] = 8$. Precipitates were aged in suspension at 60 °C for 4 h under stirring in static air and then filtered and thoroughly washed with doubly distilled water. The cake was dried at 70 °C for 12 h and again at 120 °C overnight. As-prepared HTlcs were calcined at 800 °C for 4 h to derive corresponding Co–Mg/Al mixed oxide catalysts, denoted as xCoMAO (x = 0.0, 0.5, 1.0, 1.5, 2.0, 2.5, 3.0). The oxide catalysts were then crushed, sized in 20–40 mesh for storage/reduction experiments, and kept in a desiccator to avoid reconstruction of the hydrotalcite-like structure.

Materials Characterization. The X-ray diffraction (XRD) patterns of Co–Mg/Al HT materials (xCoMA-HTs) and the derived mixed oxides (xCoMAO) were measured on a Rigaku powder diffractometer (D/MAX-RB) using Cu Kα radiation (λ = 0.15418 nm) in the 2θ range of 10–70° at a scanning rate of 4° per min. The tube voltage and current were set at 40 kV and 30 mA, respectively.

Thermal decomposition of Co–Mg/Al HTs (xCoMA-HTs) was investigated with thermogravimetry (TG, Seteram, Labsys).

In a typical measurement, 20–30 mg of HT sample was heated in an Al_2O_3 crucible at a constant heating rate of 10 °C/min from 25 to 1000 °C, with air purging at a flow rate of 30 mL/min.

The textural properties of calcined HTs (xCoMAO) were analyzed by N_2 adsorption/desorption at liquid nitrogen temperature (77 K), using a Quantachrome NOVA-1200 gas absorption analyzer. The specific surface area was calculated with the BET equation, and the pore volume and pore size distribution were obtained with the BJH method from the adsorption isotherm.

Temperature-programmed reduction (TPR) was performed for all xCoMAO catalysts on a conventional TPR apparatus equipped with a thermal conductivity detector (TCD). In general, the sample (50 mg) was inserted in a quartz tube and sandwiched between two quartz wool plugs. Prior to each TPR run, the oxide catalyst was heated to 500 °C with O_2 flushing (40 mL/min) for 30 min and then cooled to room temperature under the oxygen stream. After the flowing gas had been switched, N_2 was introduced into the reactor at 50 mL/min for 1 h at room temperature to purge away any residual oxygen. This pretreated oxide catalyst was then heated to 900 °C at a ramp of 10 °C/min and reduced in a reducing environment (5% H_2 in N_2 at a flow rate of 50 mL/min). During the heating, hydrogen consumption was monitored by the TCD.

Thermal NO_x Adsorption/Desorption. Thermal NO_x adsorption experiments were carried out in a quartz flow reactor (i.d. = 8 mm and L = 600 mm) using 1.0 g of Co–Mg/Al oxide catalyst (20–40 mesh powder). Oxide catalyst was pretreated in a gas flow of O_2/N_2 (8% O_2 by volume) at 500 °C at a constant space velocity of ~30 000 h^{-1} for 1 h and then cooled to the experimental temperature (100 or 300 °C). When the temperature had stabilized at 100 or 300 °C, 1400 ppm NO_x (1300 ppm NO and 100 ppm NO_2) and 8% O_2 in N_2 were introduced at a rate of 500 mL/min for 30 min for thermal NO_x adsorption. Concentrations of NO, NO_2, and NO_x from the reactor outlet were monitored by a Chemiluminescence NO–NO_2–NO_x analyzer (model 42C High Level, Thermo Electron Corporation).

After the thermal NO_x adsorption, the flow gas was switched to pure N_2 (rate = 500 mL/min, space velocity ≈ 30 000 h^{-1}) to flush the oxide catalyst for 20 min and remove the weakly adsorbed species at the adsorption temperature. The oxide catalyst was then cooled to 100 °C if the adsorption temperature was 300 °C. The temperature programmed desorption (TPD) was then conducted by heating the sample from 100 to 650 °C at a ramp of 10 °C per min with N_2 flowing at a rate of 500 mL/min. Concentrations of NO, NO_2, and NO_x from the reactor outlet were monitored by a chemiluminescence NO–NO_2–NO_x analyzer, and the adsorbed NO_x amount was thus calculated.

In Situ Infrared Monitoring. In situ FT-IR spectra were recorded on a Bruker Tensor 27 spectrometer in the range of 600–4000 cm^{-1} after 128 scans at a resolution of 4 cm^{-1}. Self-supporting pellets (~50 mg, 20–40 mesh) were prepared from the oxide catalysts and used directly in the IR flow cell. The IR cell, made of stainless steel, contained a KBr window and was connected to a vacuum apparatus with a residual pressure below 10^{-4} Pa. A K-type thermocouple was set in direct contact with the IR flow cell to control the temperature. Prior to the recording of an IR spectrum, the catalyst sample was pumped off for 1 h at 350 °C to eliminate impure species on the sample surface. After the sample had cooled to 100 or 300 °C under vacuum, a spectrum of the treated sample was taken as the
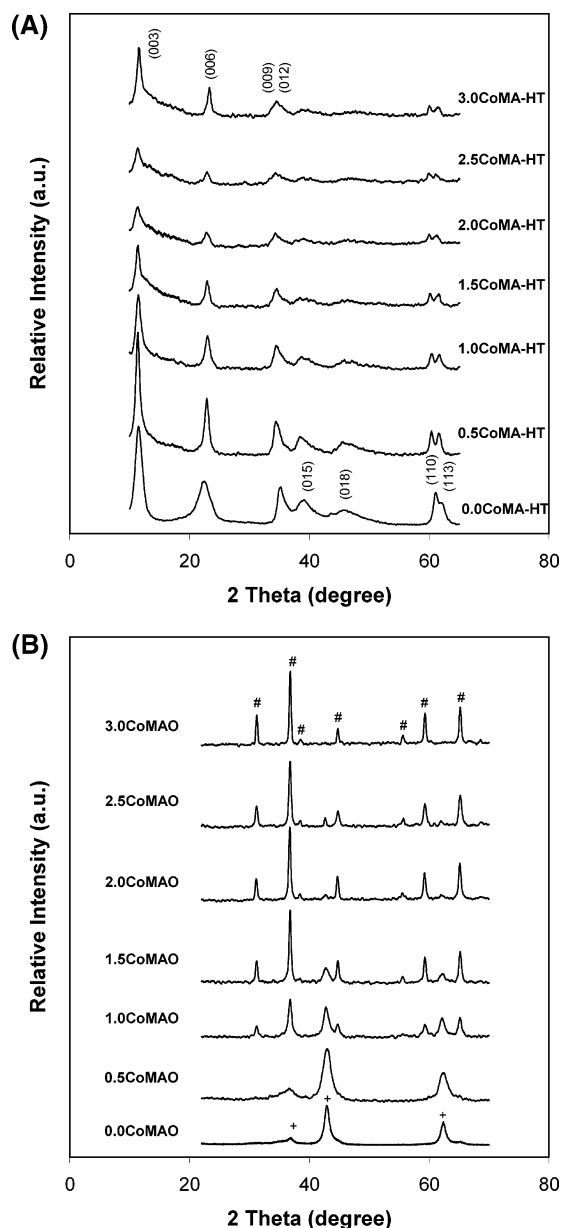
NO$_x$ Adsorption on Co−Mg/Al Hydrotalcite-like Compounds

J. Phys. Chem. B, Vol. 110, No. 9, 2006 **4293**

Figure 1. XRD patterns of (A) samples *x*CoMA-HT and (B) catalysts *x*CoMAO, where the MgO phase is marked as "+" and spinel as "#".

background at that temperature. Then, a mixture gas stream (total flow 25 mL/min) containing 1300 ppm NO, 100 ppm NO$_2$, and 8% O$_2$ in N$_2$ was introduced for NO$_x$ adsorption at 100 or 300 °C. Meanwhile, the IR spectra were sequentially recorded at the time points of 1, 2, 5, 10, 20, 30, and 60 min.

Results and Discussion

Transformation of Hydrotalcites to Mixed Oxides. As-prepared Co-containing Mg−Al hydrotalcites (*x*CoMA-HTs) are identified by the X-ray diffraction (XRD) patterns, as shown in Figure 1A. The peaks at $2\theta \approx 11°$, 22°, and 35° corresponding to the (003), (006), and (009) crystal planes, respectively, indicate relatively well-formed crystalline layered structures with rhombohedral symmetry (3R).[27,28] On the other hand, the broad diffraction peaks at ~35°, 38°, and 46° attributable to the (012), (015), and (018) crystal planes are characteristic of polytype 3R$_1$ hydrotalcites (JCPDS 22-700).[28,34,35] The well-defined (110) and (113) diffraction peaks reveal a quite good dispersion of metal ions in the hydroxide layers. The cell parameters *a* and *c*
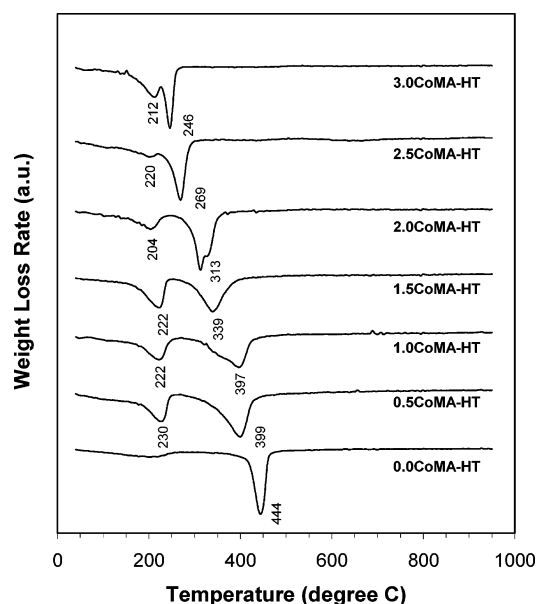

Figure 2. DTG profiles of catalysts *x*CoMAO in air.

for all HT samples are 0.306−0.309 and 2.29−2.37 nm, respectively, in good agreement with the reported values.[27] The incorporation of Co into hydroxide layers seems to affect the crystallinity of the HT crystallites. In particular, the characteristic diffraction peaks of samples 2.0CoMA-HT and 2.5CoMA-HT are much weaker and broader, probably because of the slight incompatibility of Mg and Co in the ionic size (0.072 nm for Mg^{2+} vs 0.065 nm for Co^{2+}).[28]

The XRD patterns of the derived mixed oxides (Figure 1B) show the complete transformation from the hydrotalcite to the oxide phase. It is obvious that the gradual replacement of Mg with Co in the hydrotalcite structure leads to the gradual changes in the phase composition. For sample 0.0CoMAO, i.e., Mg$_3$Al oxide, three peaks at 37°, 43°, and 62° are ascribed to the MgO phase (JCPDS 43-1022, JCPDS 89-7746). The possible spinel phase (MgAl$_2$O$_4$, JCPDS 86-2258), which is normally observable at 1000 °C,[36] was not detected. In contrast, for sample 3.0CoMAO, i.e., Co$_3$Al oxide, diffraction peaks with 2θ at ~31°, 36°, 39°, 45°, 55°, 59°, and 65° were observed that are only attributed to a spinel phase (Co$_2$AlO$_4$, JCPDS 38-0814; CoAl$_2$O$_4$, JCPDS 82-2246; Co$_3$O$_4$, JCPDS 74-2120)[37] and could be chemically expressed as Co$^{II}_{4/3}$Co$^{III}_{5/3}$AlO$_{16/3}$. This formula is supported by the TPR results (refer to section 3.2), suggesting that over half of Co^{II} ions are oxidized to Co^{III} during calcination in static air. For all tertiary oxides, both MgO and spinel are detected by XRD (Figure 1B). When more Co is incorporated to replace Mg in the hydroxide layers, the derived oxide contains more spinel and less MgO. For example, 0.5CoMAO is mainly composed of a MgO phase with an unnoticeable spinel phase, whereas samples 2.0CoMAO and 2.5CoMAO contain very minor amounts of MgO phase. This observation suggests that introduction of Co into the hydrotalcite promotes the formation of the spinel phase in the oxide catalyst, which is believed to affect the activity for NO$_x$ storage, conversion, and decomposition, as discussed shortly. In addition, the crystallite size of the spinel phase (20−25 nm) is roughly 2−3 times larger than that of the MgO phase (7−10 nm), as estimated from the peak width using the Debye−Scherrer equation.[38]

Figure 2 presents the weight loss rates of these HT compounds during heating in air, revealing the transformation of these *x*CoMA-HTs into the corresponding oxides. In general, the thermal decomposition (weight loss) of the hydrotalcites consists

TABLE 1: Textual Properties and NO$_x$ Adsorption Data of the Oxide Catalysts

sample	SSA (m^2/g)	pore volume (cm^3/g)	pore size (nm)	100 °C (mg/g)	300 °C (mg/g)
0.0CoMAO	162.7	0.47	11.6	4.15	2.57
0.5CoMAO	157.8	0.44	11.1	6.65	4.14
1.0CoMAO	83.5	0.30	14.2	5.99	4.70
1.5CoMAO	55.3	0.24	17.2	5.22	4.96
2.0CoMAO	41.2	0.22	21.0	5.91	5.90
2.5CoMAO	21.6	0.13	24.8	5.61	5.90
3.0CoMAO	21.6	0.13	23.7	4.10	3.43

of two steps. The first step occurs at 100−250 °C, and the maximum rate of weight loss is found at 210−220 °C for all HT samples, mainly ascribed to the loss of interlayer and adsorbed water molecules.[36] The second step of the weight loss at 250−500 °C consists of dehydroxylation of interlayer hydroxyl groups and decomposition of interlayer carbonate and nitrate (if any), resulting in the collapse of the layered structure.[36,37] The corresponding differential thermal gravimetry (DTG) peak moves to a lower temperature from sample 0.0CoMA-HT to sample 3.0CoMA-HT, i.e., the HT structure is destabilized upon incorporation of cobalt into the hydroxide layers. This is understandable given that Mg(OH)$_2$ is thermally more stable than Co(OH)$_2$[37,39,40] and is also reflected by the second peak temperatures of 0.0CoMA-HT (Mg$_3$Al HT, 444 °C) and 3.0CoMA-HT (Co$_3$Al HT, 246 °C) in air (Figure 2). It is known that the decomposition of carbonate takes place at 250−600 °C.[36] However, the major weight loss in the second step for all samples occurs only around the peak temperature (±20−30 °C). This could suggest that carbonate decomposition might be catalyzed by the incorporated cobalt in some way. In addition, for sample 3.0CoMA-HT, Co−OH is partially dehydroxylated in the first step[39] as the two steps are partially overlapped (Figure 2). This, together with the oxidation of Co^{II} to Co^{III} in air during the collapse facilitates the formation of the spinel phase and thermally destabilizes xCoMA-HT compounds.[41]

The BET surface area and pore volume are listed in Table 1 for the oxide catalysts derived from the corresponding HTlcs at 800 °C in air. Both the surface area and the pore volume of these oxide catalysts decrease with increasing cobalt content, as more spinel phase (big crystallites) is formed after calcination (Figure 1B). On the contrary, the average pore size between the crystallites increases. In particular, the pore size distribution (not shown here) indicates that all pores are over 2 nm, and thus, gas molecule diffusion in these pores is not the rate-determining step for adsorption and desorption.

TPR Analysis of xCoMAO Catalysts. The reduction profiles of xCoMAO samples are shown in Figure 3. It is very clear that the reduction behaviors of these catalysts are strongly related to the Co content in the oxide catalysts. For 0.0CoMAO, i.e., Mg$_3$Al oxide, no reduction peaks were detected until 900 °C, as expected. The positive baseline over 100 °C might be caused by the impurity in the experimental setup. For all other Co-containing oxide catalysts, reduction of cobalt proceeds largely in two stages, i.e., in the temperature ranges below and above 600 °C. Obviously, the reduction over 600 °C predominates in the TPR process, and the peak temperature decreases with increasing Co content, e.g., from 2.0CoMAO (870 °C) to 2.5CoMAO (820 °C) to 3.0CoMAO (730 °C). Even though we did not record data for samples 0.5-, 1.0-, and 1.5CoMAO below 900 °C, similar trends could be expected. This stabilization effect of Mg on Co reduction is presumably attributed to the good dispersion of Co in the MgAl oxide matrix that obstructs
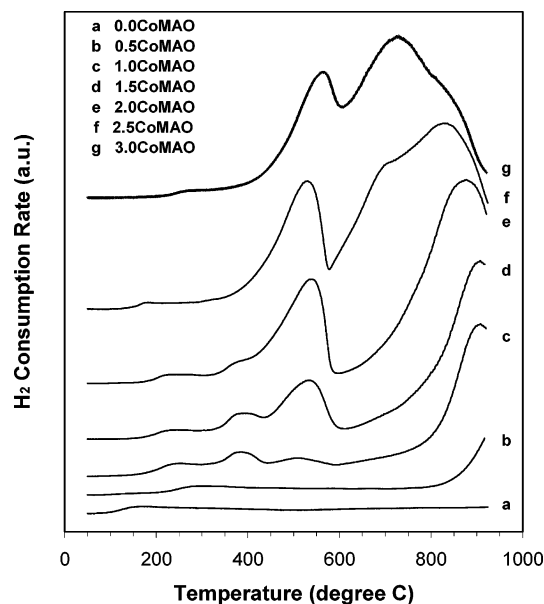
Figure 3. TPR profiles of catalysts xCoMAO in H$_2$.

hydrogen from readily accessing the cobalt ions and delays the Co(II or III) reduction.

The low-temperature reduction below 600 °C involves three small steps. The Co reduction starts around 150−200 °C and continues to 300 °C at a relatively small magnitude. Between 300 and 450 °C, there is a reduction slightly stronger than the former one (except for 0.5CoMAO). The major reduction below 600 °C occurs at 450−600 °C (except for 0.5- and 1.0CoMAO). The peak temperature slightly increases from 510 to 570 °C from sample 1.0CoMAO to 2.5CoMAO, probably because of the difficulty in H$_2$ approaching Co in larger spinel crystallites in samples containing higher levels of Co.

Because the final TPR compound for Co-containing oxide catalysts should be Co(metal)/MgAl oxide, it is reasonable to assign the high-temperature process to the reduction of bulky Co^{II} cations dispersed in spinel and MgO.[42] On this basis, we can assign the process at 510−570 °C to the reduction of bulky Co^{III} cations in the spinel and MgO phases. As suggested, sample 3.0CoMAO has a formula of Co$^{II}_{4/3}$Co$^{III}_{5/3}$AlO$_{16/3}$, so its reduction processes could be

$$Co^{II}_{4/3}Co^{III}_{5/3}AlO_{16/3} \rightarrow Co^{II}_3AlO_{9/2} \rightarrow Co(metal)/AlO_{3/2}$$
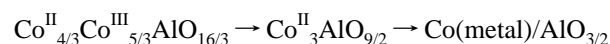
and the H$_2$ consumption ratio in these two stages should be 5/3:6, i.e., 0.278. As calculated from the TPR profile, the real H$_2$ consumption ratio at 400−590 and 590−900 °C is 0.302 for catalyst 3.0CoMAO. Bearing in mind that some Co^{II} is still not reduced when the sample is heated to 900 °C (curve g in Figure 3), the data agree well, supporting the assignments proposed above. In addition, two more minor steps at 150−300 and 300−450 °C could be assigned to reduction of surface Co^{III} and Co^{II} on spinel and/or MgO, respectively, as these cations are very easily accessed by H$_2$ and readily reduced.[36,43] The total consumption of H$_2$ in these two minor steps is about 3.4% from the TPR profile of 3.0CoMAO, in acceptable agreement with the surface amount of Co (4.8%) as estimated from the surface area in a previous report.[44]

NO$_x$ Adsorption on xCoMAO Catalysts. The adsorption profiles of NO$_x$ on samples 0.0CoMAO, 1.5CoMAO, and 3.0CoMAO at 100 and 300 °C are presented in Figure 4. As expected, NO$_x$ was adsorbed in the initial stage, as almost no NO$_x$ was detected in the outlet stream. This adsorption lasted
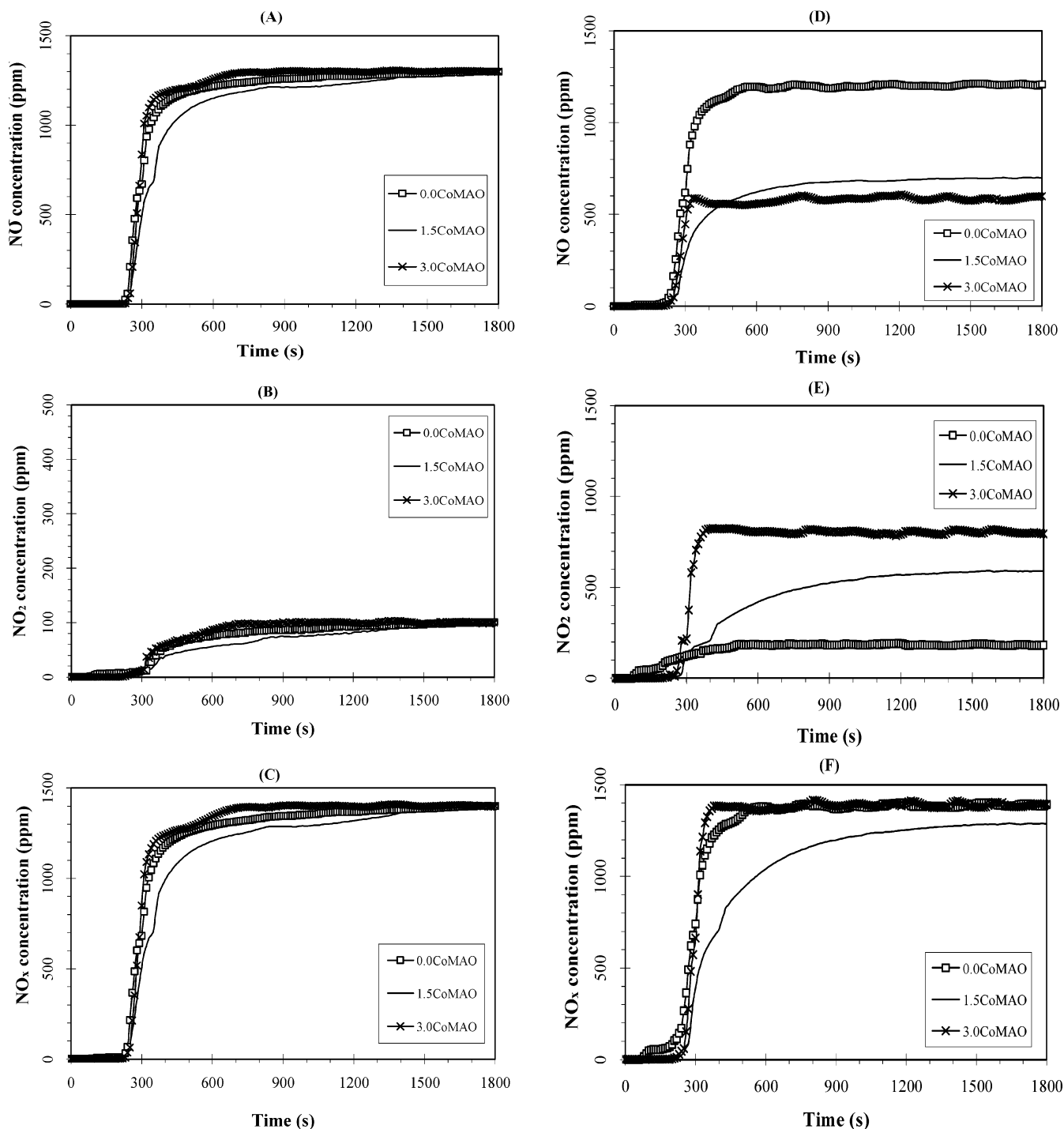
NO$_x$ Adsorption on Co−Mg/Al Hydrotalcite-like Compounds

J. Phys. Chem. B, Vol. 110, No. 9, 2006 **4295**

Figure 4. NO$_x$ adsorption on catalysts 0.0-, 1.5-, and 3.0CoMAO at (A−C) 100 and (D−F) 300 °C.

for 250 s, and then the NO$_x$ concentrations gradually recovered. At 100 °C, the NO concentration recovered to 1200−1300 ppm and the NO$_2$ concentration to 90−100 ppm after 600 s for catalysts 0.0CoMAO and 3.0CoMAO (Figure 4A−C). Under the same conditions, the adsorption on catalyst 1.5CoMAO continues to slowly trap NO$_x$ for 1500 s.

At 300 °C, the adsorption behavior of catalyst 0.0CoMAO for NO$_x$ is similar to that at 100 °C, with a slightly higher NO$_2$ concentration (180 ppm) and a slightly lower NO concentration (1200 ppm) in the later adsorption period. However, other catalysts give much different gas compositions in the outlet stream. For example, catalyst 3.0CoMAO (Co$_3$Al oxide) increases NO$_2$ concentration from 100 ppm in the feed stream to 800 ppm in the outlet stream while decreasing the NO

concentration from 1300 to 600 ppm after adsorption for about 350 s. This change in NO and NO$_2$ concentrations indicates the conversion of NO to NO$_2$ during passage through the Co$_3$-Al oxide catalyst. A similar phenomenon was observed for all of the other catalysts. Catalyst 1.5CoMAO, as an example, gradually recovered the concentrations of NO, NO$_2$, and NO$_x$ to 700, 590, and 1290 ppm, respectively after 1200 s of adsorption. The conversion from NO to NO$_2$, i.e., the increase in NO$_2$ amount, is plotted in Figure 5 (▲). It can be noted that catalysts 0.0CoMAO and 0.5CoMAO (lower Co loadings) increase the NO$_2$ concentration by only 80−100 ppm while the other catalysts increase the NO$_2$ concentration by 400−800 ppm.

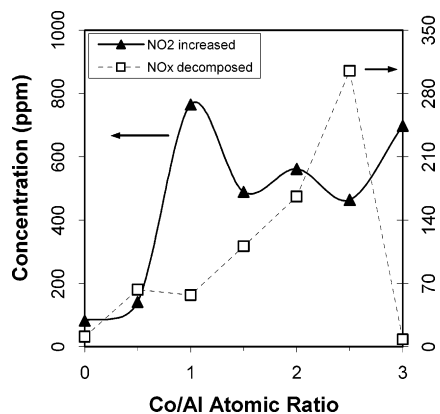Another interesting observation is that the recovered NO$_x$ concentration from catalyst 1.5CoMAO at 300 °C is always

Figure 5. NO_2 increase and NO_x decomposition at 300 °C.

TABLE 2: NO_x Desorption in Two Steps

sample	temperature range (°C)		$DeNO_x(L)/DeNO_x(H)$	
	L	H	100 °C	300 °C
0.0CoMAO	100−435	435−650	2.37	0.65
0.5CoMAO	100−290	290−600	0.54	0.01
1.0CoMAO	100−280	280−600	0.46	0.02
1.5CoMAO	100−280	280−600	0.42	0.15
2.0CoMAO	100−280	280−600	0.15	0.01
2.5CoMAO	100−330	330−650	0.53	0.05
3.0CoMAO	100−295	295−550	0.55	0.05

lower than that in the feed stream (1400 ppm). This suggests the partial decomposition of NO and/or NO_2 to other kinds of nitrogen compounds (such as N_2O, N_2)[9] that were not detected by the chemiluminescence $NO-NO_2-NO_x$ analyzer, as well as the continuous adsorption of NO_x on the catalysts. The latter seems not as likely because the adsorption is completed within 1500 s at 100 °C for all catalysts. The decomposed amount of NO_x is significantly affected by the Co loading in the tertiary catalysts, reaching a maximum of 300 ppm for catalyst 2.5CoMAO, as shown in Figure 5 (□). In comparison, binary catalysts (0.0CoMAO and 3.0CoMAO) decompose a limited amount of NO_x (about 10 ppm).

The adsorption (storage) data for NO_x on xCoMAO samples at 100 and 300 °C were calculated from the desorption profile (refer to the next section) and are listed in Table 1. Note that, at both temperatures, the storage capacity of NO_x on three-component catalysts xCoMAO (0 < x <3) is higher than that on two-component catalysts xCoMAO (x = 0 or 3). As expected, the adsorption amount of NO_x at the higher temperature (300 °C) is less than that at the lower temperature (100 °C), except for catalysts 2.0- and 2.5CoMAO.

NO_x Desorption from xCoMAO Catalysts. The desorption profiles of NO_x from typical catalysts (0.0-, 1.5-, and 3.0Co-MAO) with storage of NO_x at 100 and 300 °C are shown in Figure 6. In general, NO_x desorption seems to follow a two-step process in the temperature range of 100−650 °C. In the case of the non-Co-containing catalyst (0.0CoMAO), the desorption modes of NO_x adsorbed at 100 and 300 °C are quite similar, as can be seen from parts N and R of Figure 6 (□), only with different magnitudes in the two steps peaked at 310−330 and 520−540 °C, respectively. The ratio of the amounts of NO_x desorbed in these two steps [$DeNO_x(L)/DeNO_x(H)$, Table 2] is 2.37 at 100 °C and 0.65 at 300 °C. This could suggest that NO_x interacts with the catalyst in two different ways, where the weaker interaction characterizes various types of nitrites (corresponding to the desorption at 310−330 °C) and the stronger one represents various types of nitrates (corresponding to the desorption at 520−540 °C), as discussed in the following

section. Obviously, the predominant desorbed species from catalyst 0.0CoMAO is NO. Similarly, the desorption of NO_x from catalyst 3.0CoMAO that was adsorbed at 100 °C underwent two similar steps, one at 255 °C and the other at 355 °C, whereas these two steps occurred at much lower temperatures and over a much narrower temperature range (Figure 6 and Table 2), presumably because of the catalytic activity of cobalt for NO_x desorption. Interestingly, the NO_x absorbed at 300 °C on this catalyst desorbed only in the second step at about 360 °C ([$DeNO_x(L)/DeNO_x(H)$ = 0.05, Table 2], suggesting that there are mainly strongly bound NO_x species, i.e., various nitrates, on the catalyst surface, as addressed in the following sections.

All other tertiary catalysts, represented by 1.5CoMAO as an example, undergo a similar desorption process. However, the two stages shift to lower temperatures by about 100 °C when compared to those of catalyst 0.0CoMAO (Figure 6 and Table 2). Table 2 also indicates that the desorbed amount of NO_x adsorbed at 100 °C in the first step is only about one-half or less than that desorbed in the second step, suggesting that Co-containing catalysts either prefer the strong binding with NO_x or convert the weakly bound nitrites to strongly bound nitrates. This preference is more obvious for desorption of NO_x adsorbed at 300 °C as the desorbed NO_x in the first step can be ignored, meaning the nitrites formed on these catalysts are limited. In addition, the desorbed amount of NO_2 is comparable to that of NO for these Co-containing catalysts, unlike the case where NO is predominant in non-Co-containing catalyst 0.0CoMAO, further suggesting that the major adsorbed NO_x species are nitrates.

Species Formed on xCoMAO Catalysts. The storage/decomposition mechanism of NO_x on catalysts xCoMAO can be revealed from the species formed during the adsorption/desorption process. As described in the previous sections, NO and NO_2 are all adsorbed in the initial adsorption stage, and then their concentrations in the outlet stream are recovered back to a certain level, suggesting that the adsorption/desorption process reaches a steady equilibrium. At 300 °C, in particular, the NO_2 concentration in the outlet stream (180−870 ppm) is much higher than that in the feed (100 ppm), whereas the NO concentration (500−1200 ppm) is much lower than that in the feed (1300 ppm), indicating an apparent conversion of NO to NO_2. Moreover, the NO_x total concentration in the outlet stream from tertiary catalysts (0.5CoMAO−2.5CoMAO) is much lower than the supplied 1400 ppm, revealing the decomposition of NO_x, probably to N_2, O_2, and N_2O, on these catalysts. All of these gaseous species could be evolved through the desorption process, although N_2, O_2, and N_2O were not directly determined in this research.

On the other hand, the adsorbed species are indicated by the in situ infrared spectra of the NO_x-adsorbing catalysts. Briefly, they are various nitrites and nitrates, as well as some other nitrogen species, as summarized in Table 3. Their relative amounts, i.e., the IR peak intensities, are dependent on the adsorption time, the adsorption temperature, and the catalyst composition. As shown in Figure 7A for catalyst 0.0CoMAO (Mg_3Al oxide) as an example, the strong peak, initially located at 1246 cm^{-1} and then slightly shifted to 1263 cm^{-1}, is attributed to bridging bidentate nitrite, due to the adsorption of NO.[7,11,16,45] The other major band, initially located at 1709 cm^{-1} and later split into a broad band at 1641−1688 cm^{-1}, belongs to bridging bidentate nitrate, attributed to NO_2 adsorption.[7,11,16] Some other species, such as monodentate nitrite, linear nitrite, and monodentate nitrate, which exhibit IR peaks at 1300−1500 cm^{-1},[7,11,16]
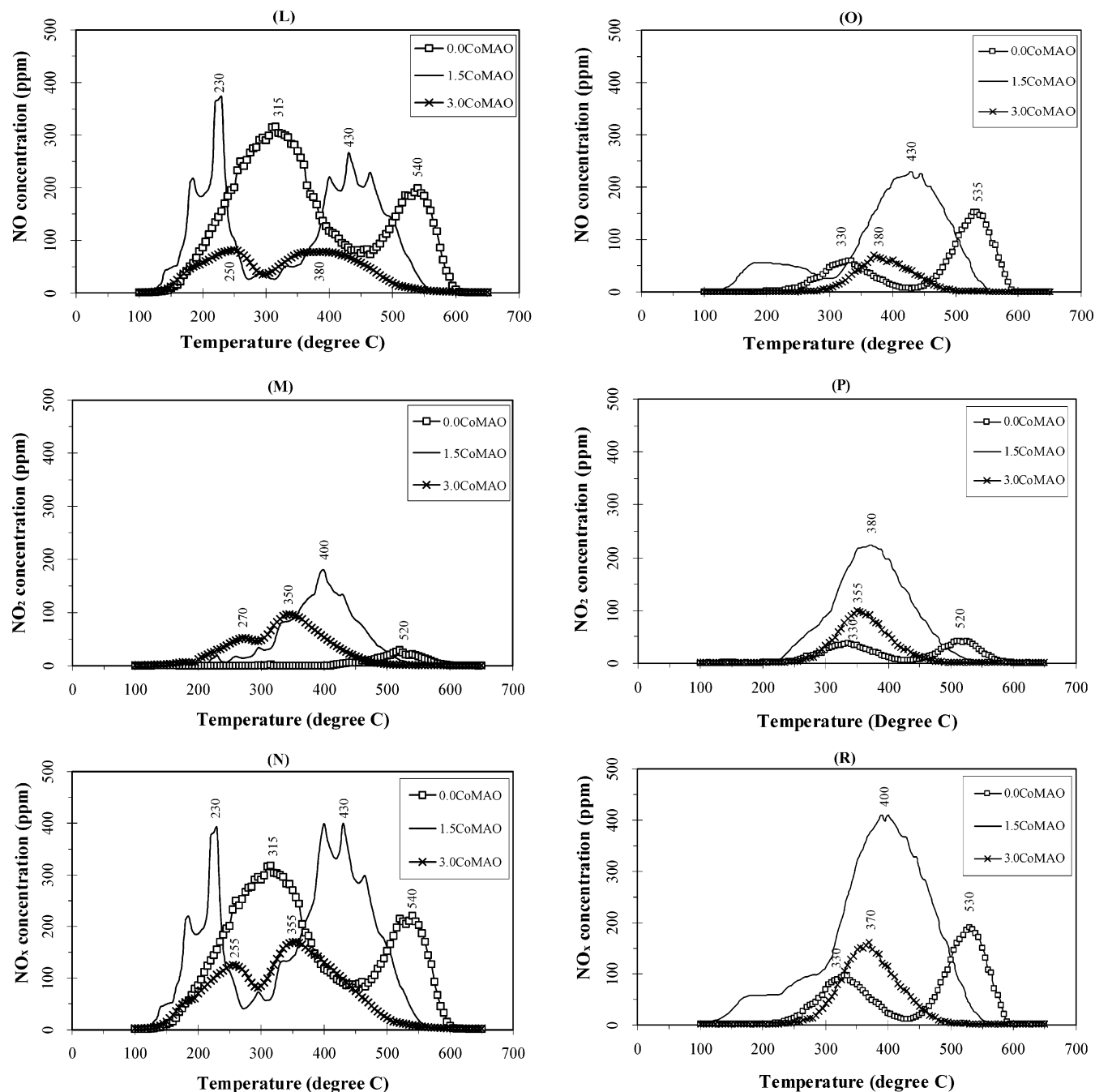
NO$_x$ Adsorption on Co−Mg/Al Hydrotalcite-like Compounds

J. Phys. Chem. B, Vol. 110, No. 9, 2006 **4297**

Figure 6. NO$_x$ desorption profile on 0.0-, 1.5-, and 3.0CoMAO at (L−N) 100 and (O−R) 300 °C.

as well as possibly N$_2$O$_2{}^{2-}$ (1400 cm^{-1}),[16] N$_2$O (adsorbed, 2009 cm^{-1}),[9] and NO$^+$ (solid, 2332−2355 cm^{-1})[46−48] are also present, (Table 3). The species adsorbed at 300 °C (Figure 7B) are quite similar, only with a lower magnitude.

Similarly, for catalyst 1.5CoMAO (Co$_{1.5}$Mg$_{1.5}$Al oxides, Figure 8A), the peak at 1649−1636 cm^{-1} becomes stronger, indicating more bridging bidentate nitrates formed than for catalyst 0.0CoMAO. The initial peak at 1228−1240 cm^{-1} due to the adsorption of NO and assigned to bridging bidentate nitrite shifts to 1308 cm^{-1} as the strongest peak in the later adsorption stage that could be assigned to monodentate nitrate (also showing a peak at 1034 cm^{-1}),[7,11,16] suggesting a redox conversion from bridging bidentate nitrite to monodentate nitrate in the presence of Co oxide. The other pronounced peak located at 1470 cm^{-1} belongs to the linear nitrite from adsorption of NO in the presence of Co oxide.[16] For adsorption at 300 °C on

catalyst 1.5CoMAO (Figure 8B), monodentate nitrate (1276, 1480, and 1048 cm^{-1}) is the major species, with some other possible minor species such as bridging bidentate nitrite (1276 cm^{-1}),[7,11,16] adsorbed N$_2$O$_4$ (1726−1732 cm^{-1}),[46] chelating bidentate nitrate (1553 and 1276 cm^{-1}), and NO$^+$ (2343 cm^{-1}).[46−48]

The species adsorbed on catalyst 3.0CoMAO (Co$_3$Al oxide) are mainly various nitrates. For example, the adsorption of NO$_x$ at 100 °C (Figure 9A) gives bridging bidentate [1628 (strongest), 1196 cm^{-1}], monodentate (1429, 1345, 1011 cm^{-1}) and chelating bidentate (1511, 1290 cm^{-1}) nitrates.[7,11,16] The time-dependent spectra (Figure 9A) clearly indicate that bridging bidentate nitrate (1628 cm^{-1}) is gradually formed and become the major species in the final stage. However, this nitrate is almost gone for 300 °C adsorption, with some monodentate (1445 and 1354 cm^{-1}) and chelating bidentate (1543−1583
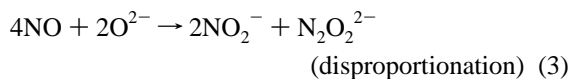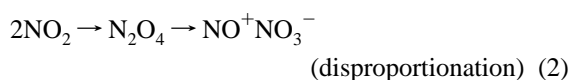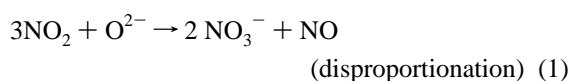
TABLE 3: Characteristic Vibrations of Adsorbed NO_x Species on xCoMAO Catalysts

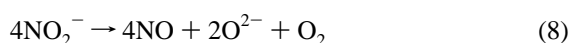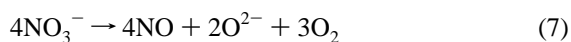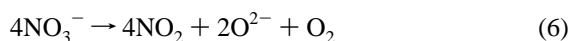| Structure	NO_x species	Mg_3Al-oxide		$Co_{1.5}Mg_{1.5}Al$-oxide		Co_3Al-oxide		Vibration
		100 °C	300 °C	100 °C	300 °C	100 °C	300 °C	
	Linear nitrite			1464-1471	1477-1480			ν(N=O)
	Bridged bidentate nitrite	1246-1263	1234-1261	1228-1240	1276	1196-1222		$\nu(NO_2,s)$ $\nu(NO_2, as)$
	Monodentate nitrite			1464-1470 1308				ν(N=O) ν(N-O)
	Bridged bidentate nitrate	1636-1688	1630-1678	1636-1649 1308		1614-1632 1345	1637-1680 1360-1377	ν(N=O) $\nu(NO_2, as)$
	Monodenate nitrate	1440-1450	1450-1462	1464-1471 1308 1034	1477-1483 1276 1048-1058	1429 1345 1020	1445-1454 1360-1377	$\nu(NO_2, as)$ $\nu(NO_2,s)$ $\nu(NO_3,s)$
	Chelating bidentate nitrate				1548-1553 1276	1511 1290-1304	1540-1595	ν(N=O) $\nu(NO_2, as)$
$(N_2O)_{ad}$	Adsorbed N_2O		2009			2081		ν(N=N)
$(NO)^+$	Nitrosonium	2353-2355 2559	2332 2532	2343		2315 2573	2322	ν(N=O)
$(N_2O_4)_{ad}$	Adsorbed N_2O_4				1726-1732	1735-1753	1732-1781	ν(N=O)
$(N_2O_2)^{2-}$	hyponitrite	1400-1500	1400-1500			1345		ν(N-O)

cm^{-1}) nitrates remaining. The other major species corresponding to the IR peaks at 1741 and 1781 cm^{-1} could be determined as adsorbed N_2O_4 (or $NO^+NO_3^-$),[46] together with peaks at 2322 (NO^+) and 1300−1500 cm^{-1} (NO_3^-) that can be also noted in the adsorption at 100 °C.

Effect of Cobalt on Adsorption/Desorption. As presented previously, Mg_3Al oxide catalyst can adsorb and store NO_x as various nitrites and nitrates that can be decomposed back to NO and NO_2 during the desorption.
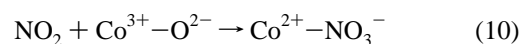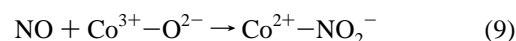
(a) adsorption

$$3NO_2 + O^{2-} \rightarrow 2 NO_3^- + NO$$
$$\text{(disproportionation) (1)}$$

$$2NO_2 \rightarrow N_2O_4 \rightarrow NO^+NO_3^-$$
$$\text{(disproportionation) (2)}$$

$$4NO + 2O^{2-} \rightarrow 2NO_2^- + N_2O_2^{2-}$$
$$\text{(disproportionation) (3)}$$

$$4NO_2 + O_2 + 2O^{2-} \rightarrow 4NO_3^- \quad (4)$$

$$4NO + O_2 + 2O^{2-} \rightarrow 4NO_2^- \quad (5)$$

(b) desorption

$$4NO_3^- \rightarrow 4NO_2 + 2O^{2-} + O_2 \quad (6)$$

$$4NO_3^- \rightarrow 4NO + 2O^{2-} + 3O_2 \quad (7)$$

$$4NO_2^- \rightarrow 4NO + 2O^{2-} + O_2 \quad (8)$$

When the adsorption/desorption reaches a steady state, the apparent NO_2 and NO concentrations do not change. The oxygen produced in reactions 6−8 could coordinate the oxidation of NO into NO_2^- and NO_2 into NO_3^-, as shown in reactions 4 and 5.

As cobalt is incorporated into the catalyst, similarly to Cu and Pt, some adsorption reactions are catalytically accelerated, leading to more NO_x adsorbed (Table 1). In particular, the following redox reactions probably take place much more quickly than reactions 4 and 5

$$NO + Co^{3+}-O^{2-} \rightarrow Co^{2+}-NO_2^- \quad (9)$$

$$NO_2 + Co^{3+}-O^{2-} \rightarrow Co^{2+}-NO_3^- \quad (10)$$

where surface Co^{3+} (or Co^{2+}) acts as the oxidant that can facilitate the adsorption of NO and NO_2. As we found that cobalt-containing oxide starts reduction in H_2 stream at 150−200 °C, so reactions 9 and 10 take place in NO_x adsorption at 300 °C. In contrast, the presence of Co can also facilitate the decomposition of nitrites and nitrates. The catalytic activities of cobalt oxide for adsorption and desorption seem to be similar in magnitude, as we note that the NO_x adsorption amount of catalyst 3.0CoMAO (Co_3Al oxide) is quite similar to that of catalyst 0.0CoMAO (Mg_3Al oxide) at 100−300 °C (Table 1). However, the tertiary catalysts can take up much more NO_x (Table 1). It is suggested that higher NO_x adsorption is due to a migration process of NO_3^- and NO_2^- from Co to adjacent Mg/Al to form relatively stable Mg/Al nitrates and nitrites.[12,49] Therefore, a careful tradeoff between Co and Mg/Al in the oxide structure and composition might lead to a powerful NO_x adsorbent catalyst, such as 2.5CoMAO, which shows a rather high NO_x adsorption at 300 °C that is comparable to that of perovskites at the same temperature.[10]

The presence of cobalt in the catalysts also causes a significant conversion of NO to NO_2 and a noticeable decomposition of NO_x at 300 °C, as shown in Figure 5. It is known that NO_x (mainly NO) is catalytically decomposed on transition metal oxides, probably to N_2 and O_2.[9,12,17,30] The as-produced oxygen can enhance the apparent conversion of NO to NO_2 via (i)

NO$_x$ Adsorption on Co−Mg/Al Hydrotalcite-like Compounds

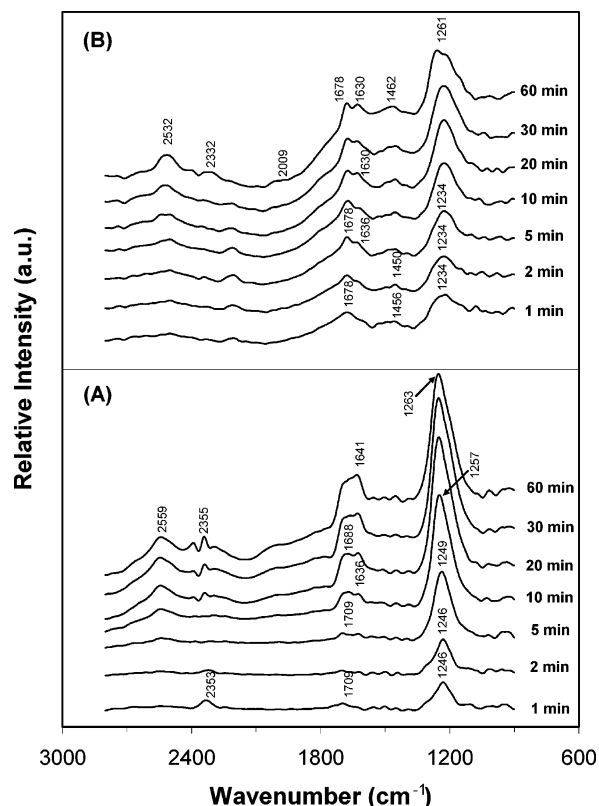*J. Phys. Chem. B, Vol. 110, No. 9, 2006* **4299**

Figure 7. In situ IR spectra of NO$_x$ adsorption on catalyst 0.0CoMAO at (A) 100 and (B) 300 °C.
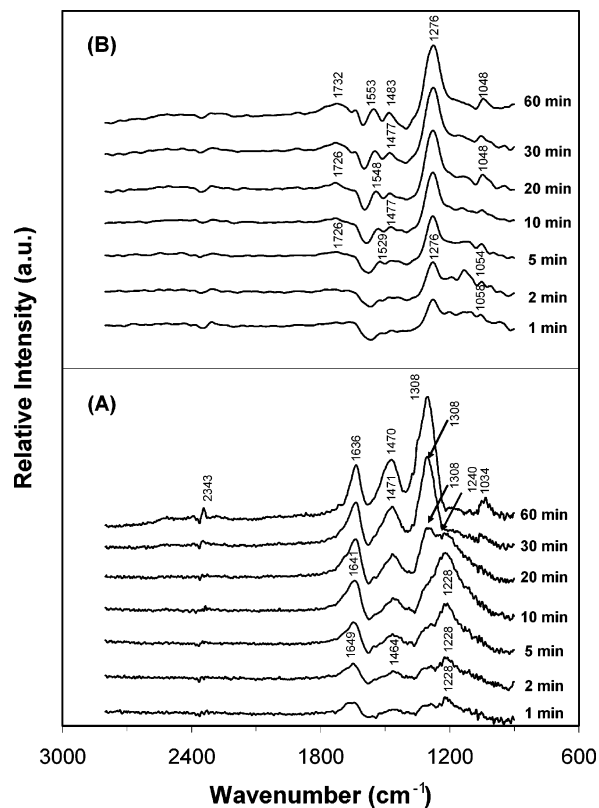

Figure 8. In situ IR spectra of NO$_x$ adsorption on catalyst 1.5CoMAO at (A) 100 and (B) 300 °C.

reaction 5 to form more nitrites and/or (ii) reaction 11 to convert more nitrites to nitrates
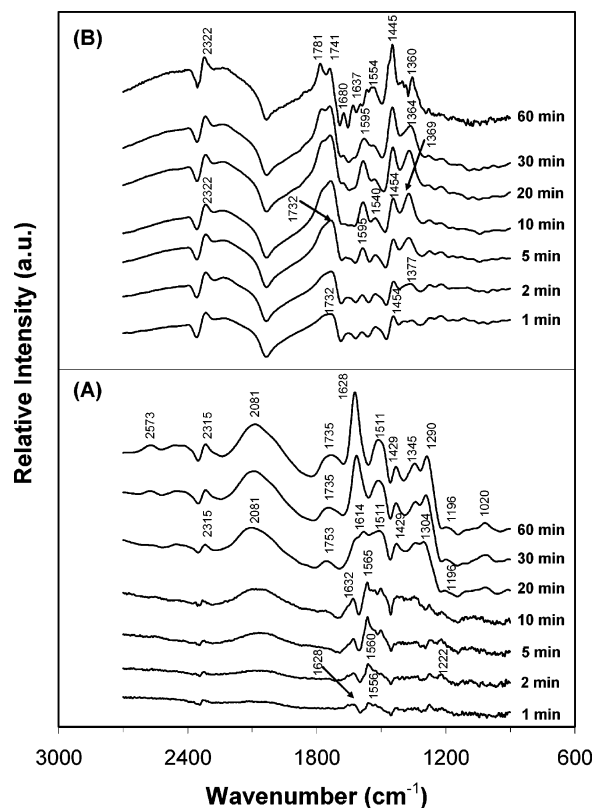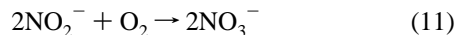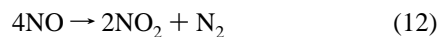
$$2NO_2^- + O_2 \rightarrow 2NO_3^- \qquad (11)$$


Figure 9. In situ IR spectra of NO$_x$ adsorption on catalyst 3.0CoMAO at (A) 100 and (B) 300 °C.

Then, the nitrates decompose to give NO$_2$. The overall stoichiometric reaction is

$$4NO \rightarrow 2NO_2 + N_2 \qquad (12)$$

This could account for the NO$_2$ concentration increase by 50−150 ppm. Most of the increase in the NO$_2$ concentration from NO is suggested to be due to the direct oxidation of NO$_2^-$ to NO$_3^-$ by the supplied O$_2$ on the Co oxide surface, as shown in reaction 11. Other possible reactions that could account for the conversion are

$$Co^{2+}-(NO_2^-)_2 \rightarrow Co^0 + 2NO_2 \qquad (13)$$

$$Co^{2+}-NO_2^- + O^{2-} \rightarrow Co^0 + NO_3^- \qquad (14)$$
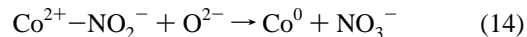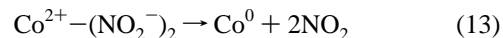
These reactions might also be responsible for the comparable NO$_2$ amounts desorbed from 100 to 650 °C in comparison to NO for Co-containing catalysts adsorbing at 300 °C (Figure 6O−R). In addition, these reactions could also take place during 100 °C adsorption and subsequent desoprtion, although the degree could be very minimal and unnoticeable for some reactions.

Conclusions

Co−Mg/Al hydrotalcite-like compounds were prepared via a coprecipitation process and identified by their XRD patterns. Their transformation to mixed oxides upon calcination was also confirmed by XRD patterns and TG analysis. The more cobalt incorporated, the more spinel phase formed, which influences the NO$_x$ adsorption/decomposition. The surface areas of the derived oxides (xCoMAO) decreased from 162.7 to 21.6 m^2/g with increasing Co content from $x = 0.0$ to $x = 3.0$.

The investigation of the reduction behaviors of *x*CoMAO catalysts indicates that the surface cobalt cations (Co^{II} and Co^{III}) were first reduced by H_2 at 150−450 °C, and then the reductions of the bulky Co^{III} to Co^{II} (450−600 °C) and the bulky Co^{II} to Co^0 (>600 °C) took place. The storage capacities of NO_x for tertiary catalysts were higher than those for binary catalysts, with 0.5CoMAO adsorbing the most NO_x (6.6 mg/g) at 100 °C and 2.0CoMAO and 2.5CoMAO adsorbing the most NO_x (5.9 mg/g) at 300 °C. During the NO_x adsorption at 300 °C on the tertiary catalysts, the catalytic conversion from NO to NO_2 and the catalytic decomposition of NO_x were observed. The in situ IR spectra suggest that the major adsorbed species are various nitrites and nitrates, with some minor species such as $N_2O_2^{2-}$, N_2O_4 (or $NO^+NO_3^-$), and N_2O. However, the relative amounts of these species depend on the catalyst composition and the adsorption temperature. On the basis of the various adsorbed species, an adsorption/desorption mechanism has been discussed. Cobalt oxide has been proposed to facilitate the oxidation of NO to nitrites and nitrates that move to adjacent Mg/Al oxide to be more stably stored in the tertiary catalysts, revealing that carefully balancing the adsorption and storage by controlling the Co/Mg ratio in the current system could lead to an optimum absorbent catalyst for NSR.

References and Notes

(1) Taylor, K. *Catal. Rev.-Sci. Eng.* **1993**, *35*, 457.

(2) Zwinkels, M. M.; Jara, S. G.; Menon, P. G. *Catal. Rev.-Sci. Eng.* **1993**, *35*, 319.

(3) Heck, R. M.; Ferrauto, R. J. *Catalytic Air Pollution Control*; Van Nostrand Reinhold: New York, 1995.

(4) Shelef, M. *Chem. Rev.* **1995**, *95*, 209.

(5) Matsumoto, S. *Catal. Today* **1996**, *29*, 43.

(6) Shinjoh, H.; Takahashi, N.; Yokota, K.; Sugiura, M. *Appl. Catal. B* **1998**, *15*, 189.

(7) Prinetto, F.; Ghiotti, G.; Nova, I.; Lietti, L.; Tronconi, E.; Forzatti, P. *J. Phys. Chem. B* **2001**, *105*, 12732.

(8) Olsson, L.; Persson, H.; Fridell, E.; Skoglundh, M.; Andersson, B. *J. Phys. Chem. B* **2001**, *105*, 6895.

(9) Garin, F. *Appl. Catal. A* **2001**, *222*, 183.

(10) Hodjati, S.; Vaezzadeh, K.; Petit, C.; Pitchon, V.; Kiennemann, A. *Appl. Catal. B* **2000**, *26*, 5.

(11) Su, Y.; Amiridis, M. D. *Catal. Today* **2004**, *96*, 31.

(12) Centi, G.; Arena, G. E.; Perathoner, S. *J. Catal.* **2003**, *216*, 443.

(13) Huang, H. Y.; Long, R. Q.; Yang, R. T. *Energy Fuels* **2001**, *15*, 205.

(14) Karen, S. K.; Rachel, L. M.; Michael, P. H. *Catal. Today* **2004**, *96*, 79.

(15) Uy, D.; Wiegand, K. A.; O'Neill, A. E.; Dearth, M. A.; Weber, W. H. *J. Phys. Chem. B* **2002**, *106*, 387.

(16) Sedlmair, Ch.; Seshan, K.; Jentys, A.; Lercher, J. A. *J. Catal.* **2003**, *214*, 308.

(17) Centi, G.; Fornasari, G.; Gobbi, C.; Livi, M.; Trifirò F.; Vaccari, A. *Catal. Today* **2002**, *73*, 287.

(18) Fornasari, G.; Trifirò, F.; Vaccari, A.; Prinetto, F.; Ghiotti, G.; Centi, G. *Catal. Today* **2002**, *75*, 421.

(19) Yamazaki, K.; Takahashi, N.; Shinjoh, H.; Sugiura, M. *Appl. Catal. B* **2004**, *53*, 1.

(20) Hodjati, S.; Petit, C.; Pitchon, V.; Kiennemann, A. *Appl. Catal. B* **2001**, *30*, 247.

(21) Li, X. G.; Chen, J. F.; Lin, P. Y.; Meng, M.; Fu, Y. L.; Tu, J.; Li, Q. X. *Catal. Commun.* **2004**, *5*, 25.

(22) Brilhac, J.-F.; Sultana, A.; Gilot, P.; Martens, J. A. *Environ. Sci. Technol.* **2002**, *36*, 1136.

(23) Sultana, A.; Habermacher, D. D.; Kirschhock, C. E. A.; Martens, J. A. *Appl. Catal. B* **2004**, *48*, 65.

(24) Szanyi, J.; Kwak, J. H.; Moline, R. A.; Peden, C. H. F. *Phys. Chem. Chem. Phys.* **2003**, *5*, 4045.

(25) Fornasari, G.; Glöckler, R.; Livi, M.; Vaccari, A. *Appl. Clay Sci.* **2005**, *29*, 258.

(26) Palomares, A. E.; López-Nieto, J. M.; Lázaro, F. J.; López A.; Corma A.; *Appl. Catal. B* **1999**, *20*, 257.

(27) Cavani, F.; Triro, F.; Vaccari, A. *Catal. Today* **1991**, *11*, 173.

(28) Braterman, P. S.; Xu, Z. P.; Yarberry, F. In *Handbook of Layered Materials*; Auerbach S. M., Carrado, K. A., Dutta, P. K., Eds.; Marcel Dekker: New York, 2004; p 373.

(29) Montanari, B.; Vaccari, A.; Gazzano, M.; Kapner, P.; Papp, H.; Dziembaj, R.; Makowski, W.; Łojewski, T.; Dziembaj, R. *Appl. Catal. B* **1996**, *16*, 205.

(30) Kang, S. F.; Jiang, Z.; Hao, Z. P. *Acta Phys. Chim. Sin.* **2005**, *21*, 278.

(31) Yu, J. J.; Jiang, Z.; Kang, S. F.; Hao, Z. P.; Hu, C. *Chin. Chem. Phys.* **2005**, *18*, 251.

(32) Corma, A.; Palomares, A. E.; Marquez, F. *J. Catal.* **1997**, *170*, 132.

(33) Shannon, I. J.; Rey, F.; Sankar, G.; Thomas, J. M.; Maschmayer, T.; Waller, A. W.; Palomares, A. E.; Corma, A.; Dent, A. J.; Greaves, G. N. *J. Chem. Soc.* **1996**, *92*, 4331.

(34) Bookin, A. S.; Drits, V. A. *Clays Clay Miner.* **1993**, *41*, 551.

(35) Xu, Z. P.; Lu, G. Q. *Chem. Mater.* **2005**, *17*, 1055.

(36) Chmielarz, L.; Kustrowski, P.; Rafalska-Lasocha, A.; Dziembaj, R. *Thermochim. Acta* **2003**, *395*, 225.

(37) Xu, Z. P.; Zeng, H. C. *J. Phys. Chem. B* **2000**, *104*, 10206.

(38) Cullity, B. D. *Elements of X-ray Diffraction*, 2nd ed.; Addison-Wesley: Reading, MA, 1978; p 278.

(39) Xu, Z. P.; Zeng, H. C.: *J. Mater. Chem.* **1998**, *8*, 2499.

(40) Halikia, I.; Economacou, A. *Int. J. Chem. Kinet.* **1993**, *25*, 609.

(41) Xu, Z. P.; Zeng, H. C. *Chem. Mater.* **2000**, *12*, 3459.

(42) Arnoldy, P.; Moulijn, J. A. *J. Catal.* **1985**, *93*, 38.

(43) Shanmugam, Y.; Lin, F.-Y.; Chang, T.-H.; Yeh, C.-T. *J. Phys. Chem. B* **2003**, *107*, 1044.

(44) In a sphere model of spinel crystallites, the ratio of the surface cobalt to the total cobalt is estimated as follows: $Co_{surface} = V_{surface}/V = (4\pi r^2 t)/(4\pi r^3/3) = 3t/r = 4.8\%$, for $r = 25$ nm (particle radius) and $t = 0.40$ nm (two Co−O bond lengths, the thickness of surface Co).

(45) Nova, I.; Castoldi, L.; Lietti, L.; Tronconi, E.; Forzatti, P.; Prinetto, F.; Ghiotti, G. *J. Catal.* **2004**, *222*, 377.

(46) Perdana, I.; Creaser, D.; Ohrman, O.; Hedlund, J. *J. Catal.* **2005**, *234*, 219.

(47) Cotton, F. A.; Wilkinson, G.; Murillo, C. A.; Bochmann, M. *Advanced Inorganic Chemistry*; John Wiley & Sons: New York, 1999; p 326

(48) Nakamoto, K. *Infrared and Raman Spectra of Inorganic and Coordinate Compounds*; John Wiley & Sons: New York, 1997; Part A, pp 160 and 166.

(49) Paterson, A. J.; Rosenberg, D. J.; Anderson, J. A. *Stud. Surf. Sci. Catal.* **2001**, *138*, 429.